

1 **Fire-climate interactions through aerosol radiative effect in a global chemistry-climate-**
2 **vegetation model**

3 Chenguang Tian^{1, 2}, Xu Yue¹, Jun Zhu¹, Hong Liao¹, Yang Yang¹, Yadong Lei³, Xinyi Zhou¹, Hao
4 Zhou², Yimain Ma², Yang Cao²

5 ¹ Jiangsu Key Laboratory of Atmospheric Environment Monitoring and Pollution Control,
6 Collaborative Innovation Center of Atmospheric Environment and Equipment Technology, School
7 of Environmental Science and Engineering, Nanjing University of Information Science &
8 Technology (NUIST), Nanjing, 210044, China

9 ² Climate Change Research Center, Institute of Atmospheric Physics, Chinese Academy of Sciences,
10 Beijing, 100029, China

11 ³ State Key Laboratory of Severe Weather & Key Laboratory of Atmospheric Chemistry of CMA,
12 Chinese Academy of Meteorological Sciences, Beijing, 100081, China

13

14 **Corresponding author:** Xu Yue (Email: yuxu@nuist.edu.cn)

15

16 **Abstract**

17 Fire emissions influence radiation, climate, and ecosystems through aerosol radiative effects.
18 ~~Meanwhile, these instantaneous environmental perturbations can~~ These can drive rapid atmospheric
19 and land surface adjustments which feed back to affect fire emissions. However, the magnitude of
20 such feedback remains unclear on the global scale. Here, we quantify the impacts of fire aerosols
21 on ~~climate~~ radiative forcing and the fast atmospheric response through direct, indirect, and albedo
22 effects based on the two-way simulations using a well-established chemistry-climate-vegetation
23 model. Globally, fire emissions cause a reduction of $0.565 \pm 0.166 \text{ W m}^{-2}$ in net radiation at the top
24 of the atmosphere with dominant contributions by aerosol indirect effect (AIE). Consequently,
25 terrestrial surface air temperature decreases by $0.061 \pm 0.165 \text{ }^\circ\text{C}$ with coolings of $>0.25^\circ\text{C}$ over
26 eastern Amazon, western U.S., and boreal Asia. Both aerosol direct effect (ADE) and AIE contribute
27 to such cooling while the aerosol albedo effect (AAE) exerts an offset warming, especially at high
28 latitudes. Land precipitation decreases by $0.180 \pm 0.966 \text{ mm month}^{-1}$ ($1.78 \pm 9.56\%$) mainly due to
29 the inhibition in central Africa by AIE. Such rainfall deficit further reduces regional leaf area index
30 (LAI) and lightning ignitions, leading to changes in fire emissions. Globally, fire emissions reduce
31 by 2%-3% because of the fire-induced fast responses in humidity, lightning, and LAI. The fire
32 aerosol radiative effects may cause larger perturbations to climate systems with likely more fires
33 under global warming.

34

35 **Short summary**

36 We quantify the impacts of fire aerosols on climate through direct, indirect, and albedo effects.
37 ~~We~~ In atmosphere-only simulations, we find global fire aerosols cause surface cooling ~~of surface air~~
38 ~~temperature~~ and rainfall inhibition ~~of precipitation over many land regions~~. These ~~climate~~ fast
39 atmospheric perturbations further ~~reduce~~ lead to a reduction in regional leaf area index and lightning
40 ~~ignitions, both of which are not beneficial for activities~~. By considering the feedback of fire aerosols
41 on humidity, lightning, and leaf area index, we predict a slight reduction in fire emissions.

42

43 **Keywords:** Fire emissions; radiative effect; climate feedback; ModelE2-YIBs model

44

45 1 Introduction

46 Fire occurs all year round in both hemispheres, burning about 1% of the Earth's surface and
47 emitting roughly 2–3 Pg (=10¹⁵ g) carbon into atmosphere every year (van der Werf *et al.*, 2017).
48 Fire activities are strongly influenced by fuel availability, ignition/suppression, and climate
49 conditions (Flannigan *et al.*, 2009). The fuel type, continuity, and amount affect fire occurrence and
50 spread probability (Flannigan *et al.*, 2013). Lightning discharge is the most important natural source
51 of fire ignition (Macias Fauria and Johnson, 2006). Human activities affect fire patterns by adding
52 ignition sources or by suppressing processes (Andela *et al.*, 2017). Compared to the above factors,
53 climate shows a more dominant role in modulating fire activities through the changes of fuel
54 moisture and spread conditions (Flannigan and Harrington, 1988).

55 Fire exerts prominent impacts on Earth systems and human society through various processes.
56 Biomass burning emits a large amount of trace gases and aerosol particles into the troposphere,
57 affecting air quality at the local and downwind regions (Yue and Unger, 2018). *In situ* observations
58 showed that about one-third of the background particles in the free troposphere of North America
59 were originated from biomass burning (Hudson *et al.*, 2004). Extremely intense fires can even inject
60 aerosols into stratosphere, where the particles were transported globally (Yu *et al.*, 2019). Fire-
61 induced air pollution can reduce global terrestrial productivity of unburned forests (Yue and Unger,
62 2018), leading to weakened carbon uptake by ecosystems. The global transport of fire air pollution
63 also causes large threats to public health by increasing the risks of diseases and mortality (Liu *et al.*,
64 2015). It is estimated that fire-induced particulate matter causes more than 33,000 deaths globally
65 each year (Chen *et al.*, 2021).

66 Aerosols from fires can cause substantial impact on climate via radiative effect owing to their
67 different optical and chemical properties (Xu *et al.*, 2021). Aerosol radiative effect ~~is the~~
68 ~~instantaneous radiative impact on energy balance of climate system, representing~~represents the fast
69 atmospheric adjustment or response before changing global mean surface air temperature (TAS).
70 First, aerosols scatter and/or absorb solar radiation through aerosol direct effect (ADE), leading to
71 altered energy budget and climate variables (Carslaw *et al.*, 2010). There is no agreement on the
72 sign of ADE of biomass burning aerosols at the global scale. Some studies (Heald *et al.*, 2014; Veira
73 *et al.*, 2015; Zou *et al.*, 2020) predicted positive forcing while others (Ward *et al.*, 2012; Jiang *et al.*,
74 2016; Grandey *et al.*, 2016) yielded negative forcing (–0.2 to 0.2 W m⁻²), mainly because of the

75 large uncertainties in the absorption of fire-emitted black carbon (BC) (Carslaw *et al.*, 2010; IPCC,
76 2014). Second, aerosols can serve as cloud condensation nuclei (CCN) or ice nuclei to affect the
77 microphysical properties of cloud. Such aerosol indirect effect (AIE) further influences climate
78 system through the changes of cloud albedo and lifetime (Twomey, 1974; Albrecht, 1989). Globally,
79 fire aerosols account for ~30% of the total CCN (Andreae *et al.*, 2004) and the overall negative AIE
80 of fire aerosol is stronger than the ADE in magnitude (Liu *et al.*, 2014; Ward *et al.*, 2012; Jiang *et al.*,
81 2016). Third, deposition of fire-emitted BC aerosols reduces surface albedo and promotes
82 ice/snow melting, which is called aerosol albedo effect (AAE) (Hansen and Nazarenko, 2004;
83 Warren and Wiscombe, 1980). Compared with other two effects, the AAE shows more regional
84 characteristics (Kang *et al.*, 2020). These fire-induced disturbance in radiative fluxes further alter
85 meteorological and hydrologic variables, which in turn affect fire activities through the changes in
86 fuel moisture and weather conditions.

87 ~~Impact~~The impacts of fire-induced ~~instantaneous climatic perturbations to rapid adjustments~~
88 ~~on fire activities~~ ~~on activity at~~ the global scale have not been fully assessed. While observations
89 revealed fire-induced perturbations to regional climate (Bali *et al.*, 2017; Zhuravleva *et al.*, 2017),
90 its feedback to fire activities are difficult to be isolated from the influences of background climate.
91 Models provide unique tools to explore fire-climate interactions resulting from aerosol radiative
92 effect especially at the regional to global scales. However, they are not routinely included in most
93 of Earth system models. The IPCC sixth assessment report (AR6) did not provide a quantitative
94 assessment of such feedback as well (IPCC, 2021). In this study, we explore the impacts of fire
95 aerosol radiative effect on climate and the consequent feedbacks to fire emissions by using a well-
96 established fire parameterization coupled to a chemistry-climate-vegetation model ModelE2-YIBs
97 (Yue and Unger, 2015). The main objectives are (1) to isolate the radiative effects of fire aerosols
98 through ADE, AIE, and AAE processes and (2) to quantify the feedback of fire-induced
99 ~~instantaneous climate effects~~ ~~rapid adjustments~~ to fire emissions.

100

101 **2 Data and methods**

102 **2.1 Data**

103 We use the emissions from Global Fire Emission Database version 4.1s (GFED4.1s) to validate
104 the simulated fire emissions. The GFED4.1s provides monthly fire emission fluxes of various air

105 pollutants based on satellite retrieval of area burned from the Moderate Resolution Imaging
106 Spectroradiometer (MODIS) (van der Werf *et al.*, 2017). Area burned in GFED4.1s is mainly
107 derived from the MODIS burned area product (Giglio *et al.*, 2013), taking into account "small" fires
108 outside the burned area maps based on active fire detections (Randerson *et al.*, 2012). The gridded
109 fire emission dataset has a spatial resolution of $0.25^\circ \times 0.25^\circ$ and is available for every month from
110 July 1997. To compute anthropogenic ignition and suppression effects (see section 2.3), we use a
111 downscaled population density dataset from Gao (2017, 2020). Monthly sea surface temperature
112 (SST) and sea ice concentration (SIC) obtained from Hadley Centre Sea Ice and Sea Surface
113 Temperature (HadISST) dataset (Rayner *et al.*, 2003) are used as the boundary conditions for the
114 climate model.

115

116 2.2 ModelE2-YIBs model

117 The chemistry-climate-vegetation model ModelE2-YIBs is used to simulate the two-way
118 coupling between fire aerosols and climate systems. The ModelE2-YIBs is composed of the NASA
119 Goddard Institute for Space Studies (GISS) ModelE2 model (Schmidt *et al.*, 2014) and the Yale
120 Interactive terrestrial Biosphere Model (YIBs) (Yue and Unger, 2015). The GISS ModelE2 is a
121 global climate-chemistry model with a horizontal resolution of $2^\circ \times 2.5^\circ$ latitude by longitude and
122 40 vertical layers extending to the stratosphere (0.1hPa). The dynamics and physics codes are
123 executed every 30 minutes and the radiation code is calculated every 2.5 hours.

124 The gas-phase chemistry scheme considers 156 chemical reactions among 51 species,
125 including NO_x - HO_x - O_x - CO - CH_4 chemistry and different species of volatile organic
126 compounds. Aerosol species in ModelE2 include sulfate, nitrate, ammonium, sea salt, dust, BC, and
127 organic carbon (OC), which are interactively calculated and tracked for both mass and number
128 concentrations. Heterogeneous chemistry on dust surfaces and NO_x -dependent secondary organic
129 aerosol production from isoprene and terpenes is included in the model (Bauer *et al.*, 2007b;
130 Tsigaridis and Kanakidou, 2007). The thermodynamic gas-aerosol equilibrium module is used to
131 calculate the phase partitioning of the $\text{H}_2\text{SO}_4/\text{HSO}_4^- / \text{SO}_4^{2-} - \text{HNO}_3/\text{NO}_3^- - \text{NH}_3/\text{NH}_4^+$
132 $-\text{HCl}/\text{Cl}^- - \text{Na}^+ - \text{Ca}^{2+} - \text{Mg}^{2+} - \text{K}^+ - \text{H}_2\text{O}$ system (Metzger *et al.*, 2006; Bauer *et al.*, 2007a). The
133 aerosol microphysical scheme is based on the quadrature method of moments, which incorporates
134 nucleation, gas-particle mass transfer, new particle formation, particle emissions, aerosol phase

135 chemistry, condensational growth, and coagulation (Bauer *et al.*, 2008). The residence time of
136 aerosol species varies greatly in space and time due to different removal rates. Turbulent dry
137 deposition is determined by resistance-in-series scheme, which is closely coupled to the boundary
138 layer scheme and implemented between the surface layer (10 m) and the ground (Koch *et al.*, 2006).
139 The wet deposition consists of several processes including scavenging within and below cloud,
140 evaporation of falling rainout, transportation along convective plumes, and detrainment and
141 evaporation from convective plumes (Koch *et al.*, 2006; Shindell *et al.*, 2006).

142 In ModelE2, gases can be converted to aerosols through chemical reactions, while aerosols
143 affect photolysis and provide reaction surface for gases. For example, the formation of sulfate
144 aerosols is driven by modeled oxidants (Bell *et al.*, 2005), and the chemical production of nitrate
145 aerosols is dependent on nitric acid and gaseous ammonia (~~Bauer *et al.*, 2007~~)(~~Bauer *et al.*, 2007b~~).
146 Moreover, the disturbances of aerosols on climate systems via direct, indirect, and albedo effects
147 are considered in ModelE2. ~~Size-dependent Aerosol~~ optical parameters ~~of aerosols~~ are calculated by
148 the Mie scattering theory using complex refractive index depending on chemical speciation and
149 particle size. The first AIE is estimated by the prognostic treatment of cloud droplet number
150 concentration, which is a function of species-dependent contact nucleation, auto-conversion, and
151 immersion freezing (Menon *et al.*, 2008; Menon *et al.*, 2010). The AAE of BC is considered by
152 estimating the decline of surface albedo as a function of aerosol concentrations at the top layer of
153 snow or ice (Koch and Hansen, 2005). We note that average BC content in deposition to snow is
154 determined/estimated by measurement-based average scavenging ratios is used as a climatological
155 proxy to the physical process of BC deposition (Hansen and Nazarenko, 2004). The latter
156 involves size resolved and meteorologically dependent BC deposition fluxes, as would be found
157 in a chemical transport model, but is not used here due to computational constraints. More
158 detailed descriptions of ModelE2 can be found in Schmidt *et al.* (2014). It has been extensively
159 evaluated for meteorological and chemical variables against observations, reanalysis products and
160 other models, and widely used for studies of climate systems, atmospheric components, and their
161 interactions (Schmidt *et al.*, 2014).

162 YIBs is a process-based vegetation model that dynamically simulates tree growth and
163 terrestrial carbon fluxes with prescribed fractions of nine plant functional types (PFTs), including
164 deciduous broadleaf forest, evergreen needleleaf forest, evergreen broadleaf forest, tundra,

165 shrubland, C₃/C₄ grassland, and C₃/C₄ cropland. Essential biological processes such as
 166 photosynthesis, phenology, autotrophic and heterotrophic respiration are considered and
 167 parameterized using the state-of-the-art schemes (Yue and Unger, 2015). Dynamic daily leaf area
 168 index (LAI) is estimated based on carbon allocation which is updated every 10 days and prognostic
 169 phenology which is dependent instantaneously on temperature and drought conditions. Simulated
 170 tree height, phenology, gross primary productivity and LAI agree well with site-level observations
 171 and/or satellite retrievals (Yue and Unger, 2015). The YIBs model joined the dynamic global
 172 vegetation model inter-comparison project TRENDY and showed reasonable performance of
 173 carbon fluxes against available observations (Friedlingstein *et al.*, 2020). In the coupled model,
 174 ModelE2 provides meteorological drivers to YIBs, which feeds back to alter land surface water and
 175 energy fluxes through changes in stomatal conductance, surface albedo, and LAI. By incorporating
 176 YIBs into ModelE2, the new coupled model ModelE2-YIBs can simulate interactions between
 177 terrestrial ecosystems and climate systems through the exchange of water and energy fluxes, and
 178 chemical components (Yue and Unger, 2015; Yue *et al.*, 2017).

179

180 **2.3 Fire parameterization**

181 We implemented the active global fire parameterization from Pechony and Shindell (2009) into
 182 ModelE2-YIBs model. The parameterization considers key fire-related processes including fuel
 183 flammability, lightning and human ignitions, and human suppressions. Flammability is a unitless
 184 metric indicating conditions favorable for fire occurrence, and is calculated using vapor pressure
 185 deficit (VPD, hPa), precipitation (R, mm day⁻¹), and LAI (m² m⁻²) as follows:

$$186 \quad \text{Flam} = \text{VPD} \times \text{LAI} \times e^{-C_R \times R} \quad (1)$$

187 Here, LAI represents vegetation density and is dynamically calculated by YIBs model. C_R is a
 188 constant set to 2. VPD is a vital indicator of flammability conditions:

$$189 \quad \text{VPD} = e_s \times \left(1 - \frac{\text{RH}}{100}\right) \quad (2)$$

190 where e_s is the saturation vapor pressure and RH is surface relative humidity. e_s can be
 191 calculated by Goff-Gratch equation:

$$192 \quad e_s = e_{st} \times 10^Z \quad (3)$$

193 where e_{st} is 1013.246 hPa and

194
$$Z = a \times \left(\frac{T_s}{T} - 1 \right) + b \times \log \frac{T_s}{T} + c \times \left(10^{d \left(1 - \frac{T_s}{T} \right)} - 1 \right) + f \times \left(10^{h \left(\frac{T_s}{T} - 1 \right)} - 1 \right) \quad (4)$$

195 Here, a, b, c, d, f and h are constants set to -7.90298, 5.02808, -1.3816×10⁻⁷, 11.344, 8.1328×10⁻³
 196 and -3.49149, respectively. T_s is boiling point of water and equal to 373.16 K. VPD and LAI in Eq.
 197 (1) are calculated in half-hourly and daily time step, respectively, while 30-day running average
 198 precipitation is employed to avoid unrealistically huge flammability fluctuations. It should be noted
 199 that the response of flammability to abovementioned factors may not be instantaneous, but may
 200 occur over time. For example, a reduction in precipitation in one season at a given location may
 201 reduce foliage growth and hence reduce the fuel available for combustion in another season.

202 Natural and anthropogenic ignition rate determines whether the fire can actually occur. If the
 203 ignition rate is zero, the resulting fire emissions will be zero, regardless of flammability. ~~Natural~~The
 204 natural ignition ~~source~~rate I_N depends on cloud-to-ground lightning (CoGL) rate, which is simulated
 205 by ModelE2 following the parameterization of Price and Rind (1994):

206
$$I_N = \text{CoGL} = \begin{cases} 3.44 \times 10^{-5} \times H^{4.9} & \text{over land} \\ 6.4 \times 10^{-4} \times H^{1.73} & \text{over ocean} \end{cases} \quad (5)$$

207 where H is the cloud depth (unit: km).

208 Humans influence fire activity by adding ignition sources and suppressing fire events, the rates
 209 of which increase with population and to some extent counteract each other. The ~~number of~~
 210 anthropogenic ignition ~~source~~rate I_A (number km⁻² month⁻¹) is calculated as follows (Venevsky *et*
 211 *al.*, 2002):

212
$$I_A = k(\text{PD}) \times \text{PD} \times \alpha \quad (6)$$

213 where PD is population density (number km⁻²). k(PD) = 6.8 × PD^{-0.6} stands for ignition
 214 potentials of human activity, assuming that people in scarcely populated areas interact more with
 215 the natural ecosystems and therefore produce more ignition potential. α is the number of potential
 216 ignitions per person per month and set to 0.03.

217 In principle, the successful suppression of fires is dependent on early detection. It is reasonably
 218 assumed that fires are detected earlier and suppressed more effectively in highly populated areas.
 219 Therefore, the fraction of non-suppressed fires F_{NS} can be expressed as:

220
$$F_{NS} = c_1 + c_2 \times \exp(-\omega \times \text{PD}) \quad (7)$$

221 where c₁, c₂ and ω are constants and set to 0.05, 0.95 and 0.05, respectively. The selection of
 222 constant values in Eq. (7) is done in a heuristic way, due to lack of quantified data globally. It

223 assumes that up to 95% of fires is suppressed in the densely populated regions but only 5% in
224 unpopulated areas.

225 With the calculation of flammability (Flam), ignition (I_N and I_A), and non-suppression (F_{NS}),
226 the fire count density N_{fire} (unit: number km^{-2}) at a specific time step can be derived as:

$$227 \quad N_{\text{fire}} = \text{Flam} \times (I_N + I_A) \times F_{NS} \quad (8)$$

228 Finally, fire emissions of trace gases and particulate matters (FireEmis) are calculated as:

$$229 \quad \text{FireEmis} = N_{\text{fire}} \times \text{EF} \quad (9)$$

230 Here, EF is the PFT-specific emission factor of an air pollutant such as BC, OC, NO_x , NH_3 , SO_2 ,
231 CO, Alkenes and Paraffin. For each species, simulated gridded emissions are grouped by dominant
232 PFT and compared to annual total emissions from GFED4.1s over the same grids. The EF is then
233 calibrated to minimize the root-mean-square error between the simulated and GFED data for all
234 land grids. Such calibration adjusts only the global total amount of fire emissions without changing
235 the spatiotemporal pattern predicted by the parameterization. The EF is the intrinsic attribution of
236 wildfire emissions that should not vary greatly with climatic conditions. The fire-emitted minerals
237 or dust-like materials are not implemented in the current model, given that these species is not
238 included in the current GFED4.1s.

239 Compared to fire indexes, such as Canadian Fire Weather Index system (Wagner, 1987), this
240 fire parameterization shows advantages in integrating the effects of meteorology, vegetation, natural
241 ignition, and human activities (both ignition and suppression) on fires. Furthermore, it is physically
242 straightforward and has been validated based on global observations (~~Pechony and Shindell,~~
243 2009);(Pechony and Shindell, 2009; Hantson *et al.*, 2020). In ModelE2-YIBs, fire emissions are
244 affected by environmental factors following above parameterizations. In turn, the radiative effects
245 of fire-emitted aerosols feed back to affect those climatic and ecological factors. Note that the
246 changes in the environmental factors may result in changes to fire emissions later. We consider
247 only the fire emissions at surface due to the large uncertainties in depicting fire plume height (Sofiev
248 *et al.*, 2012; Ke *et al.*, 2021). The fire emissions include both primary aerosols and trace gases, the
249 latter of which react with other species to form the secondary aerosols. These particles could be
250 transported across the globe by the three-dimensional atmospheric circulation and eventually
251 removed through either dry or wet deposition.

252

253 2.4 Simulations

254 We perform four groups of sensitivity experiments (Table 1) with the ModelE2-YIBs model to
255 quantify the fire-climate interactions through different radiative processes. The first group with
256 suffix ‘AD’ considers only the ADE. The second (third) group with suffix ‘AD_AI’ (‘AD_AA’)
257 considers both ADE and AIE (ADE and AAE). The fourth group with suffix ‘AD_AI_AA’ includes
258 all three aerosol radiative effects (ADE, AIE, and AAE). Within each group, two runs are performed
259 with (YF) or without (NF) fire emissions. For YF simulations, fire-induced aerosols including
260 primarily emitted and secondarily formed are dynamically calculated based on fire parameterization
261 (see section 2.3) and atmospheric transport. These fire emissions cause radiative perturbations and
262 the consequent ~~changes in climatic variables~~fast atmospheric adjustments, which ~~feedback~~feed back
263 to influence fire emissions. For NF simulations, fire emissions are calculated offline at each step
264 without perturbing the climate system, which can be considered that there is no fire emission. By
265 comparing the climatic variables from the YF and NF runs in the first group, we isolate the impacts
266 of fire aerosols on climate through ADE. By comparing the climatic effects from the first and second
267 (third) groups, we isolate the AIE (AAE) of fire aerosols. By comparing the climatic variables from
268 YF and NF runs in the fourth group, the overall effect (ADE+AIE+AAE) is obtained. Besides, the
269 differences of fire emissions between simulations of “YF_AD_AI_AA” and “NF_AD_AI_AA”
270 represent the feedback of fire aerosol-induced environmental perturbations. Note that fire-emitted
271 gas-phase species also perturb radiation via atmospheric absorption and/or feedback from rapid
272 adjustment; these perturbations are far less than aerosol forcing and could be ignored.

273 For each simulation, climatological mean CO₂ concentrations, SST/SIC, and population
274 density during 1995-2005 are used as boundary conditions to drive the model. Such configuration
275 ignores the year-to-year variability in climate systems, which may cause significant changes in
276 annual fire emissions (Burton *et al.*, 2020). Each simulation is integrated for 25 years with the first
277 5 years spinning up and the last 20 ~~year~~ years averaged. ~~Two-tail student~~A two-tailed Student t-test
278 is performed to assess 90% confidence levels of the predicted radiative and climatic responses ($p <$
279 0.1). The global mean or sum value is depicted in the form of mean value \pm standard deviation.
280 In this study, downward (upward) radiative/heat fluxes are defined as positive (negative). Given that
281 the model is driven by prescribed SST and SIC, only the rapid adjustments of atmospheric variables
282 are taken into account and we mainly focus on climate changes over land grid. The radiative effect

283 simulated with such model configuration is termed the effective radiative forcing (~~ERF~~-(IPCC,
284 2014).

286 **3 Results**

287 **3.1 Model evaluation**

288 Simulated fire emissions of BC and OC show hotspots in the tropics, such as Amazon, Sahel,
289 central Africa, and Southeast Asia (Fig. S1). The large tropical fire emissions are related to abundant
290 vegetation and/or distinct dry seasons. Compared to GFED4.1s data, ModelE2-YIBs slightly
291 underestimates boreal fire emissions especially over northern Asia and North America. On the
292 global scale, fire releases 1.85 ± 0.01 Tg ($1 \text{ Tg} = 10^{12} \text{ g}$) C year⁻¹ of BC and 16.8 ± 0.92 Tg C year⁻¹
293 of OC in ModelE2-YIBs, close to the 1.86 Tg C year⁻¹ of BC and 16.4 Tg C year⁻¹ of OC estimated
294 by GFED4.1s. In general, ModelE2-YIBs reasonably captures the spatial distribution of fire
295 emissions, with high spatial correlations of 0.67 ($p < 0.01$) for BC and 0.58 ($p < 0.01$) for OC, and
296 low normalized mean biases of 0.6% for BC and 2.4% for OC against satellite-based observations.

298 **3.2 Fire-induced radiative perturbations**

299 Fig. S2 shows the fire-induced changes in Aerosol Optical Depth (AOD) at 550nm. Fire
300 emissions largely enhance surface aerosols especially over tropical regions. Hotspots are located in
301 southern Africa and South America with regional enhancement larger than 0.05. In addition, large
302 enhancement is also found at boreal high latitudes (> 0.01). At the global scale, fires enhance AOD
303 by 0.006 ± 0.001 with 0.010 ± 0.001 over land.

304 Fire aerosols cause large perturbations in net radiation at top of atmosphere (TOA). Globally,
305 the net radiation at TOA decreases $0.565 \pm 0.166 \text{ W m}^{-2}$ by fire aerosols (Fig. 1a). Regionally,
306 negative changes are predicted over central Africa, western South America, western North America
307 and the boreal high latitudes. Diagnosis shows that fire-induced AIE dominates the reduction of
308 TOA flux with a global value of $-0.440 \pm 0.264 \text{ W m}^{-2}$ (Fig. 1c), accounting for 78% of the total
309 TOA radiative effect by fire aerosols. The spatial correlation coefficient is 0.62 over land grids
310 between the perturbations by all aerosol effects and that by AIE alone. Compared to AIE, the
311 changes in TOA radiative fluxes are much smaller for fire ADE ($-0.058 \pm 0.213 \text{ W m}^{-2}$, Fig. 1b) and
312 AAE ($-0.016 \pm 0.283 \text{ W m}^{-2}$, Fig. 1d) with limited perturbations on land.

313 Fire aerosols decrease net shortwave radiation reaching the surface up to 9 W m^{-2} in central
314 Africa and 7 W m^{-2} in Amazon (Fig. 2a), where biomass burning emissions are most intense (Fig.
315 S1). Such pattern is in general consistent with the changes of TOA fluxes (Fig. 1a), leading to an
316 average reduction of $-1.227 \pm 0.216 \text{ W m}^{-2}$ in the shortwave radiation over global land. The fire-
317 induced ADE alone reduces land surface shortwave radiation by $0.654 \pm 0.353 \text{ W m}^{-2}$ with the
318 maximum center in Amazon (Fig. S3a). As a comparison, the fire-induced AIE causes a smaller
319 reduction of $-0.553 \pm 0.518 \text{ W m}^{-2}$ with the hotspot in central Africa (Fig. S3c). The net effect of
320 AAE ($0.263 \pm 0.551 \text{ W m}^{-2}$) by fire aerosols is positive mainly because fire AAE reduces surface
321 albedo and increase shortwave radiation over Tibetan Plateau and boreal high latitudes (Fig. S3e).
322 However, the magnitude of AAE is much smaller compared to that of ADE and AIE.

323 Changes in surface longwave radiation (Fig. 2b) are much smaller than those in shortwave
324 radiation (Fig. 2a). Regionally, positive changes are predicted in the western U.S., eastern Amazon,
325 and South Africa, where fire-induced surface cooling (Fig. 3a) decreases the upward longwave
326 radiation. On the global scale, fire aerosols cause a decrease of $0.281 \pm 0.371 \text{ W m}^{-2}$ in surface
327 upward longwave radiation. As a result, fire aerosols induce a net atmospheric absorption of 0.191
328 $\pm 0.227 \text{ W m}^{-2}$ over land grids (Fig. 2c). The reductions in surface shortwave radiation are largely
329 balanced by changes in heat fluxes at the surface, which shows an average decrease of 0.826 ± 0.311
330 W m^{-2} in the upward fluxes over land grids (Fig. 2d). Fire ADE and AIE lead to reductions of 0.503
331 $\pm 0.289 \text{ W m}^{-2}$ and $0.432 \pm 0.411 \text{ W m}^{-2}$ in surface upward heat fluxes, respectively (Fig. S3b and
332 S3d). Changes in sensible heat account for 82.2 % of the changes in total heat reduction, much
333 higher than the contributions of 17.8% by latent heat fluxes (Fig. S4). Regionally, the upward
334 sensible heat decreases in the western U.S. and Amazon mainly due to fire ADE, while the upward
335 latent heat decreases in central Africa mainly by fire AIE (Fig. S5).

336

337 **3.3 Fire-induced fast climatic responses**

338 In response to the perturbations in radiative fluxes, land TAS decreases $0.061 \pm 0.165 \text{ }^{\circ}\text{C}$
339 globally by fire aerosols (Fig. 3a). Such cooling is mainly located in western U.S., Amazon, and
340 boreal Asia, following the large reductions in shortwave radiation (Fig. 2a). Meanwhile, moderate
341 warming is predicted at the high latitudes of both hemispheres especially over the areas covered
342 with land ice such as Greenland and Antarctica. Sensitivity experiments show that both ADE (Fig.

343 4a) and AIE (Fig. 4c) of fire aerosols result in net cooling globally, with regional reductions of TAS
344 over boreal Asia and North America. In contrast, the fire AAE causes increases of TAS over boreal
345 Asia and North America (Fig. 4e), where the deposition of BC aerosols reduces surface albedo.
346 Consequently, the fire AAE results in a global warming of $0.054 \pm 0.163^\circ\text{C}$, which in part offsets
347 the cooling effects by the ADE and AIE of fire aerosols.

348 Meanwhile, global land precipitation decreases by 0.180 ± 0.966 mm/month ($1.78 \pm 9.56\%$)
349 with great spatial heterogeneity (Fig. 3b). Decreased precipitation is predicted over central Africa,
350 boreal North America, and eastern Siberia. In contrast, increased rainfall is predicted in western
351 U.S., eastern Amazon, and northern Asia. The reduction of precipitation is mainly contributed by
352 fire AIE, which reduces cloud droplet size and inhibits local rainfall in central Africa (Fig. 4d).
353 Consequently, latent heat fluxes are reduced to compensate the rainfall deficit in central Africa (Fig.
354 S4b).

355

356 **3.4 ~~ClimateFast response feedback to~~ fire aerosol radiative effect emissions**

357 The fire-aerosol-induced fast response in precipitation, VPD, lightning, and LAI can feed back
358 to affect fire emissions. However, these changes may have contrasting impacts on fire activities. For
359 example, the aerosol-induced reduction of precipitation in central Africa (Fig. 3b) increases local
360 VPD (Fig. 5a) and consequently causes more fire emissions. Meanwhile, such enhanced drought
361 condition inhibits plant growth and decreases local LAI (Fig. 5c), which has negative impacts on
362 fire emissions by reducing fuel density. Furthermore, the fire AIE inhibits the development of
363 convective cloud, which limits cloud height and the number of cloud-to-ground lightning in central
364 Africa (Fig. 5b), leading to reduced ignition sources and fire emissions.

365 To illustrate the joint the impacts of fire-aerosol-induced ~~instantaneous climatic change~~
366 fast climate responses, we count the number out of the four factors contributing positive effects to fire
367 emissions over land grids (Fig. 5d). The larger (smaller) number indicates higher possibility of
368 increasing (decreasing) fire emissions. Most of areas show neutral number of 2, indicating offsetting
369 effects of the changes in fire-prone factors. Only 13.5 % of land grids show numbers higher than 2
370 with sparse distribution. In contrast, 32.1 % of land grids show numbers smaller than 2, especially
371 for the grids over Siberia and western U.S. where the increased rainfall (Fig. 3b) and decreased VPD
372 (Fig. 5a) inhibit fire emissions. Furthermore, the regional reductions in lightning ignition or LAI

373 promote the inhibition effects. As a result, fire emissions in YF_AD_AI_AA slightly decrease by
374 $31.0 \pm 35.9 \text{ Gg year}^{-1}$ (1.7%) for BC and $493.6 \pm 566.8 \text{ Gg year}^{-1}$ (2.9%) for OC compared to
375 NF_AD_AI_AA in which fire emissions do not perturb climate (Fig. 6).

376

377 **4 Conclusions and discussion**

378 We used the chemistry-climate-vegetation coupled model ModelE2-YIBs to quantify fire-
379 climate interactions through ADE, AIE, and AAE. Globally, fire aerosols decrease TOA net
380 radiation by $0.565 \pm 0.166 \text{ W m}^{-2}$, dominated by the AIE over central Africa. Surface net solar
381 radiation also exhibits widespread reductions especially over fire-prone areas with compensations
382 from the decreased sensible and latent heat fluxes. Following the changes in radiation, land TAS
383 decreases by $0.061 \pm 0.165 \text{ }^{\circ}\text{C}$ and precipitation decreases by $0.180 \pm 0.966 \text{ mm/month}$, albeit with
384 regional inconsistencies. The surface cooling is dominated by fire ADE and AIE, while the drought
385 tendency is mainly contributed by fire AIE with hotspots in central Africa. AAE also plays an
386 important role by introducing warming tendency at the mid-to-high latitudes. These fire-induced
387 fast climatic responses further affect VPD, LAI, and lightning ignitions, leading to reductions in
388 global fire emissions of BC by 2% and OC by 3%. It may seem counter-intuitive that reduced
389 precipitation would decrease wildfire emissions, while the observation-based data show that the
390 fire-precipitation correlations are not negative in all regions (Fig. S6). In this study, the inhibition
391 of precipitation in central Africa (Fig. 3b) reduces regional LAI (Fig. 5c) and decreases fuel
392 availability for fire occurrence, resulting in a positive correlation between fire and precipitation that
393 matches the observed relationship in Africa (Fig. S6). However, in North America, Eurasia, and the
394 Amazon Basin, precipitation is anti-correlated with fire emissions. These differences may reflect
395 the seasonal variation of rainfall in the different regions.

396 Our predicted reduction of $0.565 \pm 0.166 \text{ W m}^{-2}$ in TOA radiation by fire aerosols is close to
397 the estimate of -0.51 W m^{-2} reported by Jiang *et al.* (2016) and -0.59 W m^{-2} of Zou *et al.* (2020)
398 using different models with prescribed SST/SIC and fire-induced ADE, AIE and AAE (Table 2).
399 Within such change, fire ADE alone makes a moderate contribution of $-0.016 \pm 0.283 \text{ W m}^{-2}$, falling
400 within the range of -0.2 to 0.2 W m^{-2} from other studies. The large uncertainty of fire ADE is likely
401 related to the discrepancies in the BC absorption among climate models, which cause varied net
402 effects when offsetting the radiative perturbations of scattering aerosols. As a comparison, fire AIE

403 in our model induces a significant radiative effect of $-0.440 \pm 0.264 \text{ W m}^{-2}$. However, such
404 magnitude is much smaller than previous estimates of -0.7 to -1.1 W m^{-2} using different models
405 (Table 2). We further estimated a limited fire AAE of $-0.016 \pm 0.283 \text{ W m}^{-2}$, consistent with previous
406 findings showing insignificant role of AAE by fire aerosols (Ward *et al.*, 2012; Jiang *et al.*, 2016).
407 Our estimates of reductions in TAS and precipitation also fall within the range of previous studies
408 (Table 2).

409 Our estimates are subject to some limitations and uncertainties. First, we considered only the
410 fast climatic responses of land surface with prescribed SST and SIC in the simulations. Although
411 most of fire-induced AOD changes are located on land (Fig. S2), the air-sea interaction may cause
412 complex climatic responses to aerosol radiative effects. In a recent study, Jiang *et al.* (2020)
413 emphasized the role of slow feedback contributed by fire aerosols on global precipitation reduction
414 by using a coupled model. Such air-sea interaction will modify the magnitude and/or spatial pattern
415 of fast climatic responses revealed in this study, and should be explored in the future studies with
416 coupled ocean models. Second, the nonlinear effects of different radiative processes may influence
417 the attribution results. In this study, we isolate the effects of AIE and AAE by subtracting variables
418 between different groups following the approaches by Bauer and Menon (2012). However, the
419 additive perturbations from individual processes are not equal to the total perturbations with all
420 processes in one simulation. For example, the sum of three processes causes changes of TOA
421 radiation by $-0.513 \pm 0.324 \text{ W m}^{-2}$ (Figs 1b-1d), surface temperature by $-0.037 \pm 0.160 \text{ }^\circ\text{C}$ (Figs 4a,
422 4c, 4e), and precipitation by $-1.090 \pm 1.122 \text{ mm month}^{-1}$ (Figs 4b, 4d, 4f). These perturbations are
423 weaker than the net effects of $0.565 \pm 0.166 \text{ W m}^{-2}$ (Fig. 1a) in radiation and $-0.061 \pm 0.165 \text{ }^\circ\text{C}$ in
424 temperature (Fig. 3a), but much stronger than that of $-0.18 \pm 0.96 \text{ mm month}^{-1}$ in precipitation (Fig.
425 3b) predicted by the simulation with all three processes. As a result, the nonlinear feedbacks among
426 different radiative processes may magnify or offset the final climatic responses to fire aerosols.
427 Third, considering the complex nature of fire activities, the fire parameterization in this study does
428 not incorporate all fire-related processes (e.g., the influence of wind). In addition, the simulations
429 omit several factors influencing fire emissions (e.g., moist content of fuels) and aerosol radiative
430 effects (e.g. fire plume height). For example, studies show significant impacts of plume rise on the
431 vertical distribution of fire aerosols and the consequent radiative effects (Walter *et al.*, 2016). The
432 impacts of human activity on fire emissions are calculated as a function of population density

433 without considerations of differences in economy, education, and policies. These auxiliary factors
434 may increase the spatial heterogeneity of fire aerosol radiative effects and deserve further
435 explorations in the future studies.

436 Despite these limitations, we made the first attempt to assess the two-way interaction between
437 fire emissions and climate via aerosol radiative effects. Our results show that fire-emitted aerosols
438 cause negative ERF of $0.565 \pm 0.166 \text{ W m}^{-2}$, which is about 20% of the anthropogenic ERF due to
439 the increased greenhouse gases and aerosols from 1950 to 2019 (IPCC, 2021). Such fire ERF largely
440 reduces regional TAS and precipitation, leading to further changes in fire emissions. Although the
441 reduction of 2% to 3% in fire emissions by the fire-climate interaction through aerosol radiative
442 effect seems limited, such change is a result of several complex feedbacks that may exert offsetting
443 effects-, and the relative magnitude of individual factors may vary spatially. Both the number of
444 factors and the magnitude of their effects will determine the overall response. Furthermore, our
445 simulations reveal a strong inhibition effect of fire aerosols on LAI in central Africa due to the
446 aerosol-induced drought intensification. Such negative effects on ecosystems are inconsistent with
447 previous estimates that showed certain fertilization effects by fire aerosols (Yue and Unger, 2018),
448 mainly because the rainfall deficit overweighs the diffuse fertilization effects of aerosols. With likely
449 more fires under global warming (Abatzoglou *et al.*, 2019), our results suggested complex and
450 uncertain perturbations by fire emissions to climate and ecosystem through fire-climate interactions.

451

452 **Acknowledgements**

453 The authors are grateful to Dr. Matthew Kasoar and another anonymous reviewer for their
454 constructive comments that have improved this study.

455

456 **Financial support**

457 This research was supported by the National Key Research and Development Program of China
458 (grant no. 2019YFA0606802).

459

460 **Competing Interests**

461 The authors declare that they have no conflict of interest.

462

463 **Data availability**

464 Hadley Centre Sea Ice and Sea Surface Temperature dataset were obtain from
465 <https://www.metoffice.gov.uk/hadobs/hadisst/>. Population data could be downloaded form
466 <https://cmr.earthdata.nasa.gov/search/concepts/C1739468823-SEDAC.html>. GFED data were
467 obtained from https://daac.ornl.gov/VEGETATION/guides/fire_emissions_v4_R1.html. Model
468 data from this study are available from the corresponding author upon request.

469 **Reference:**

- 470 Abatzoglou J T, Williams A P and Barbero R 2019 Global Emergence of Anthropogenic Climate Change
471 in Fire Weather Indices *Geophysical Research Letters* **46** 326-36
- 472 Albrecht B A 1989 Aerosols, Cloud Microphysics, and Fractional Cloudiness **245** 1227-30
- 473 Andela N, Morton D C, Giglio L, Chen Y, van der Werf G R, Kasibhatla P S, DeFries R S, Collatz G J,
474 Hantson S, Kloster S, Bachelet D, Forrest M, Lasslop G, Li F, Mangeon S, Melton J R, Yue C
475 and Randerson J T 2017 A human-driven decline in global burned area *Science* **356** 1356
- 476 Andreae M O, Rosenfeld D, Artaxo P, Costa A A, Frank G P, Longo K M and Silva-Dias M A F 2004
477 Smoking Rain Clouds over the Amazon **303** 1337-42
- 478 Bali K, Mishra A K and Singh S 2017 Impact of anomalous forest fire on aerosol radiative forcing and
479 snow cover over Himalayan region *Atmospheric Environment* **150** 264-75
- 480 [Bauer S E, Koch D, Unger N, Metzger S M, Shindell D T and Streets D G 2007a Nitrate aerosols today
481 and in 2030: a global simulation including aerosols and tropospheric ozone *Atmos. Chem. Phys.*
482 **7** 5043-59](#)
- 483 Bauer S E and Menon S 2012 Aerosol direct, indirect, semidirect, and surface albedo effects from sector
484 contributions based on the IPCC AR5 emissions for preindustrial and present-day conditions
485 **117**
- 486 Bauer S E, Mishchenko M I, Lacis A A, Zhang S, Perlwitz J and Metzger S M ~~2007~~2007b Do sulfate and
487 nitrate coatings on mineral dust have important effects on radiative properties and climate
488 modeling? **112**
- 489 Bauer S E, Wright D L, Koch D, Lewis E R, McGraw R, Chang L S, Schwartz S E and Ruedy R 2008
490 MATRIX (Multiconfiguration Aerosol TRacker of mIXing state): an aerosol microphysical
491 module for global atmospheric models *Atmos. Chem. Phys.* **8** 6003-35
- 492 Bell N, Koch D and Shindell D T 2005 Impacts of chemistry-aerosol coupling on tropospheric ozone and
493 sulfate simulations in a general circulation model **110**
- 494 Burton C, Betts R A, Jones C D, Feldpausch T R, Cardoso M and Anderson L O 2020 El Niño Driven
495 Changes in Global Fire 2015/16 **8**
- 496 Carslaw K S, Boucher O, Spracklen D V, Mann G W, Rae J G L, Woodward S and Kulmala M 2010 A
497 review of natural aerosol interactions and feedbacks within the Earth system *Atmos. Chem. Phys.*
498 **10** 1701-37
- 499 Chen G, Guo Y, Yue X, Tong S, Gasparrini A, Bell M L, Armstrong B, Schwartz J, Jaakkola J J K,
500 Zanutti A, Lavigne E, Nascimento Saldiva P H, Kan H, Royé D, Milojevic A, Overcenco A,
501 Urban A, Schneider A, Entezari A, Vicedo-Cabrera A M, Zeka A, Tobias A, Nunes B, Alahmad
502 B, Forsberg B, Pan S-C, Íñiguez C, Ameling C, De la Cruz Valencia C, Åström C, Houthuijs D,
503 Van Dung D, Samoli E, Mayvaneh F, Sera F, Carrasco-Escobar G, Lei Y, Orru H, Kim H,
504 Holobaca I-H, Kyselý J, Teixeira J P, Madureira J, Katsouyanni K, Hurtado-Díaz M,
505 Maasikmets M, Ragettli M S, Hashizume M, Stafoggia M, Pascal M, Scortichini M, de Sousa
506 Zanotti Stagliorio Coêlho M, Valdés Ortega N, Rytí N R I, Scovronick N, Matus P, Goodman P,
507 Garland R M, Abrutzky R, Garcia S O, Rao S, Fratanni S, Dang T N, Colistro V, Huber V, Lee
508 W, Seposo X, Honda Y, Guo Y L, Ye T, Yu W, Abramson M J, Samet J M and Li S 2021
509 Mortality risk attributable to wildfire-related PM_{2.5} pollution: a global
510 time series study in 749 locations *The Lancet Planetary Health* **5** e579-e87
- 511 Flannigan M, Cantin A S, de Groot W J, Wotton M, Newbery A and Gowman L M 2013 Global wildland
512 fire season severity in the 21st century *Forest Ecology and Management* **294** 54-61

513 Flannigan M and Harrington J B 1988 A Study of the Relation of Meteorological Variables to Monthly
514 Provincial Area Burned by Wildfire in Canada (1953–80) *Journal of Applied Meteorology and*
515 *Climatology* **27** 441-52

516 Flannigan M, Krawchuk M A, de Groot W J, Wotton B M and Gowman L M 2009 Implications of
517 changing climate for global wildland fire %J *International Journal of Wildland Fire* **18** 483-507

518 Friedlingstein P, O'Sullivan M, Jones M W, Andrew R M, Hauck J, Olsen A, Peters G P, Peters W,
519 Pongratz J, Sitch S, Le Quéré C, Canadell J G, Ciais P, Jackson R B, Alin S, Aragão L E O C,
520 Arneth A, Arora V, Bates N R, Becker M, Benoit-Cattin A, Bittig H C, Bopp L, Bultan S,
521 Chandra N, Chevallier F, Chini L P, Evans W, Florentie L, Forster P M, Gasser T, Gehlen M,
522 Gilfillan D, Gkritzalis T, Gregor L, Gruber N, Harris I, Hartung K, Haverd V, Houghton R A,
523 Ilyina T, Jain A K, Joetzjer E, Kadono K, Kato E, Kitidis V, Korsbakken J I, Landschützer P,
524 Lefèvre N, Lenton A, Lienert S, Liu Z, Lombardozzi D, Marland G, Metz N, Munro D R, Nabel
525 J E M S, Nakaoka S I, Niwa Y, O'Brien K, Ono T, Palmer P I, Pierrot D, Poulter B, Resplandy
526 L, Robertson E, Rödenbeck C, Schwinger J, Séférian R, Skjelvan I, Smith A J P, Sutton A J,
527 Tanhua T, Tans P P, Tian H, Tilbrook B, van der Werf G, Vuichard N, Walker A P, Wanninkhof
528 R, Watson A J, Willis D, Wiltshire A J, Yuan W, Yue X and Zaehle S 2020 Global Carbon Budget
529 2020 *Earth Syst. Sci. Data* **12** 3269-340

530 Gao J 2017 Downscaling Global Spatial Population Projections from 1/8-degree to 1-km Grid Cells.

531 Gao J 2020 Global 1-km Downscaled Population Base Year and Projection Grids Based on the Shared
532 Socioeconomic Pathways, Revision 01. (Palisades, NY: NASA Socioeconomic Data and
533 Applications Center (SEDAC))

534 Giglio L, Randerson J T and van der Werf G R 2013 Analysis of daily, monthly, and annual burned area
535 using the fourth-generation global fire emissions database (GFED4) *Journal of Geophysical*
536 *Research: Biogeosciences* **118** 317-28

537 Grandey B S, Lee H H and Wang C 2016 Radiative effects of interannually varying vs. interannually
538 invariant aerosol emissions from fires *Atmos. Chem. Phys.* **16** 14495-513

539 Hansen J and Nazarenko L 2004 Soot climate forcing via snow and ice albedos **101** 423-8

540 [Hantson S, Kelley D I, Arneth A, Harrison S P, Archibald S, Bachelet D, Forrest M, Hickler T, Lasslop](#)
541 [G, Li F, Mangeon S, Melton J R, Nieradzik L, Rabin S S, Prentice I C, Sheehan T, Sitch S,](#)
542 [Teckentrup L, Voulgarakis A and Yue C 2020 Quantitative assessment of fire and vegetation](#)
543 [properties in simulations with fire-enabled vegetation models from the Fire Model](#)
544 [Intercomparison Project *Geosci. Model Dev.* **13** 3299-318](#)

545 Heald C L, Ridley D A, Kroll J H, Barrett S R H, Cady-Pereira K E, Alvarado M J and Holmes C D 2014
546 Contrasting the direct radiative effect and direct radiative forcing of aerosols *Atmos. Chem. Phys.*
547 **14** 5513-27

548 Hudson P K, Murphy D M, Cziczo D J, Thomson D S, de Gouw J A, Warneke C, Holloway J, Jost H-J
549 and Hübner G 2004 Biomass-burning particle measurements: Characteristic composition and
550 chemical processing **109**

551 IPCC 2014 *Contribution of Working Groups I, II and III to the Fifth Assessment Report of the*
552 *Intergovernmental Panel on Climate Change [Core Writing Team, R.K. Pachauri and L.A.*
553 *Meyer (eds.)]* (IPCC, Geneva, Switzerland)

554 IPCC 2021 *Climate Change 2021: The Physical Science Basis. Contribution of Working Group I to the*
555 *Sixth Assessment Report of the Intergovernmental Panel on Climate Change [Masson-Delmotte,*
556 *V., P. Zhai, A. Pirani, S. L. Connors, C. Péan, S. Berger, N. Caud, Y. Chen, L. Goldfarb, M. I.*

557 Gomis, M. Huang, K. Leitzell, E. Lonnoy, J. B. R. Matthews, T. K. Maycock, T. Waterfield, O.
558 Yelekçi, R. Yu and B. Zhou (eds.)] vol In Press.: Cambridge University Press.)

559 Jiang Y, Lu Z, Liu X, Qian Y, Zhang K, Wang Y and Yang X Q 2016 Impacts of global open-fire aerosols
560 on direct radiative, cloud and surface-albedo effects simulated with CAM5 *Atmos. Chem. Phys.*
561 **16** 14805-24

562 Jiang Y, Yang X-Q, Liu X, Qian Y, Zhang K, Wang M, Li F, Wang Y and Lu Z 2020 Impacts of Wildfire
563 Aerosols on Global Energy Budget and Climate: The Role of Climate Feedbacks *Journal of*
564 *Climate* **33** 3351-66

565 Kang S, Zhang Y, Qian Y and Wang H 2020 A review of black carbon in snow and ice and its impact on
566 the cryosphere *Earth-Science Reviews* **210** 103346

567 Ke Z, Wang Y, Zou Y, Song Y and Liu Y 2021 Global Wildfire Plume-Rise Data Set and
568 Parameterizations for Climate Model Applications **126** e2020JD033085

569 Koch D and Hansen J 2005 Distant origins of Arctic black carbon: A Goddard Institute for Space Studies
570 ModelE experiment *Journal of Geophysical Research: Atmospheres* **110**

571 Koch D, Schmidt G A and Field C V 2006 Sulfur, sea salt, and radionuclide aerosols in GISS ModelE
572 **111**

573 Liu J C, Pereira G, Uhl S A, Bravo M A and Bell M L 2015 A systematic review of the physical health
574 impacts from non-occupational exposure to wildfire smoke *Environmental Research* **136** 120-
575 32

576 Liu Y, Goodrick S and Heilman W 2014 Wildland fire emissions, carbon, and climate: Wildfire–climate
577 interactions *Forest Ecology and Management* **317** 80-96

578 Macias Fauria M and Johnson E A 2006 Large-scale climatic patterns control large lightning fire
579 occurrence in Canada and Alaska forest regions *Journal of Geophysical Research:*
580 *Biogeosciences* **111**

581 Menon S, Del Genio A D, Kaufman Y, Bennartz R, Koch D, Loeb N and Orlikowski D 2008 Analyzing
582 signatures of aerosol-cloud interactions from satellite retrievals and the GISS GCM to constrain
583 the aerosol indirect effect **113**

584 Menon S, Koch D, Beig G, Sahu S, Fasullo J and Orlikowski D 2010 Black carbon aerosols and the third
585 polar ice cap *Atmos. Chem. Phys.* **10** 4559-71

586 [Metzger S, Mihalopoulos N and Lelieveld J 2006 Importance of mineral cations and organics in gas-](#)
587 [aerosol partitioning of reactive nitrogen compounds: case study based on MINOS results *Atmos.*](#)
588 [*Chem. Phys.* **6** 2549-67](#)

589 Pechony O and Shindell D T 2009 Fire parameterization on a global scale *Journal of Geophysical*
590 *Research* **114**

591 Price C and Rind D 1994 Modeling Global Lightning Distributions in a General Circulation Model
592 *Monthly Weather Review* **122** 1930-9

593 Randerson J T, Chen Y, van der Werf G R, Rogers B M and Morton D C 2012 Global burned area and
594 biomass burning emissions from small fires *Journal of Geophysical Research: Biogeosciences*
595 **117**

596 Rayner N A, Parker D E, Horton E B, Folland C K, Alexander L V, Rowell D P, Kent E C and Kaplan A
597 2003 Global analyses of sea surface temperature, sea ice, and night marine air temperature since
598 the late nineteenth century **108**

599 Schmidt G A, Kelley M, Nazarenko L, Ruedy R, Russell G L, Aleinov I, Bauer M, Bauer S E, Bhat M
600 K, Bleck R, Canuto V, Chen Y-H, Cheng Y, Clune T L, Del Genio A, de Fainchtein R, Faluvegi

601 G, Hansen J E, Healy R J, Kiang N Y, Koch D, Lacis A A, LeGrande A N, Lerner J, Lo K K,
602 Matthews E E, Menon S, Miller R L, Oinas V, Oloso A O, Perlwitz J P, Puma M J, Putman W
603 M, Rind D, Romanou A, Sato M, Shindell D T, Sun S, Syed R A, Tausnev N, Tsigaridis K,
604 Unger N, Voulgarakis A, Yao M-S and Zhang J 2014 Configuration and assessment of the GISS
605 ModelE2 contributions to the CMIP5 archive *Journal of Advances in Modeling Earth Systems*
606 **6** 141-84

607 Shindell D T, Faluvegi G, Unger N, Aguilar E, Schmidt G A, Koch D M, Bauer S E and Miller R L 2006
608 Simulations of preindustrial, present-day, and 2100 conditions in the NASA GISS composition
609 and climate model G-PUCCINI *Atmos. Chem. Phys.* **6** 4427-59

610 Sofiev M, Ermakova T and Vankevich R 2012 Evaluation of the smoke-injection height from wild-land
611 fires using remote-sensing data *Atmos. Chem. Phys.* **12** 1995-2006

612 [Tsigaridis K and Kanakidou M 2007 Secondary organic aerosol importance in the future atmosphere](#)
613 [*Atmospheric Environment* **41** 4682-92](#)

614 Twomey S 1974 Pollution and the planetary albedo *Atmospheric Environment (1967)* **8** 1251-6

615 van der Werf G R, Randerson J T, Giglio L, van Leeuwen T T, Chen Y, Rogers B M, Mu M, van Marle
616 M J E, Morton D C, Collatz G J, Yokelson R J and Kasibhatla P S 2017 Global fire emissions
617 estimates during 1997–2016 *Earth Syst. Sci. Data* **9** 697-720

618 Veira A, Kloster S, Schutgens N A J and Kaiser J W 2015 Fire emission heights in the climate system –
619 Part 2: Impact on transport, black carbon concentrations and radiation *Atmos. Chem. Phys.* **15**
620 7173-93

621 Venevsky S, Thonicke K, Sitch S and Cramer W 2002 Simulating fire regimes in human-dominated
622 ecosystems: Iberian Peninsula case study *Global Change Biology* **8** 984-98

623 Wagner V 1987 *Development and structure of the Canadian Forest Fire Weather Index System, Forestry*
624 *Technical Report: Canadian Forestry Service)*

625 Walter C, Freitas S R, Kottmeier C, Kraut I, Rieger D, Vogel H and Vogel B 2016 The importance of
626 plume rise on the concentrations and atmospheric impacts of biomass burning aerosol *Atmos.*
627 *Chem. Phys.* **16** 9201-19

628 Ward D S, Kloster S, Mahowald N M, Rogers B M, Randerson J T and Hess P G 2012 The changing
629 radiative forcing of fires: global model estimates for past, present and future *Atmos. Chem. Phys.*
630 **12** 10857-86

631 Warren S G and Wiscombe W J 1980 A Model for the Spectral Albedo of Snow. II: Snow Containing
632 Atmospheric Aerosols %J *Journal of Atmospheric Sciences* **37** 2734-45

633 Xu L, Zhu Q, Riley W J, Chen Y, Wang H, Ma P-L and Randerson J T 2021 The Influence of Fire
634 Aerosols on Surface Climate and Gross Primary Production in the Energy Exascale Earth
635 System Model (E3SM) *Journal of Climate* **34** 7219-38

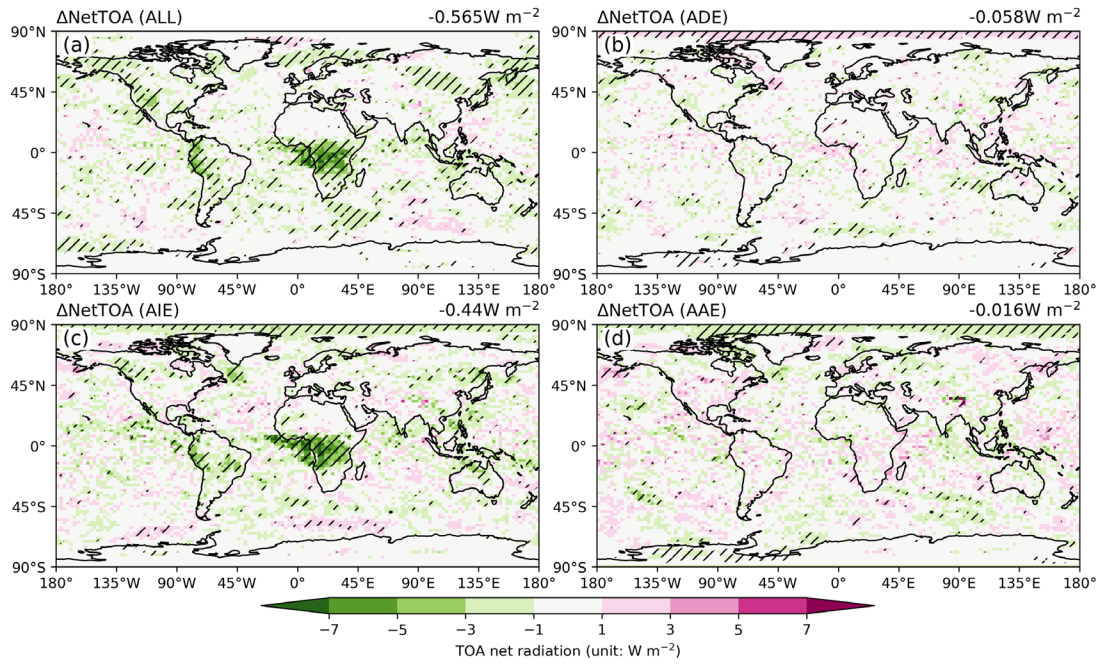
636 Yan H, Zhu Z, Wang B, Zhang K, Luo J, Qian Y and Jiang Y 2021 Tropical African wildfire aerosols
637 trigger teleconnections over mid-to-high latitudes of Northern Hemisphere in January
638 *Environmental Research Letters* **16** 034025

639 Yu P, Toon O B, Bardeen C G, Zhu Y, Rosenlof K H, Portmann R W, Thornberry T D, Gao R-S, Davis S
640 M, Wolf E T, Gouw J d, Peterson D A, Fromm M D and Robock A 2019 Black carbon lofts
641 wildfire smoke high into the stratosphere to form a persistent plume **365** 587-90

642 Yue X, Strada S, Unger N and Wang A 2017 Future inhibition of ecosystem productivity by increasing
643 wildfire pollution over boreal North America *Atmos. Chem. Phys.* **17** 13699-719

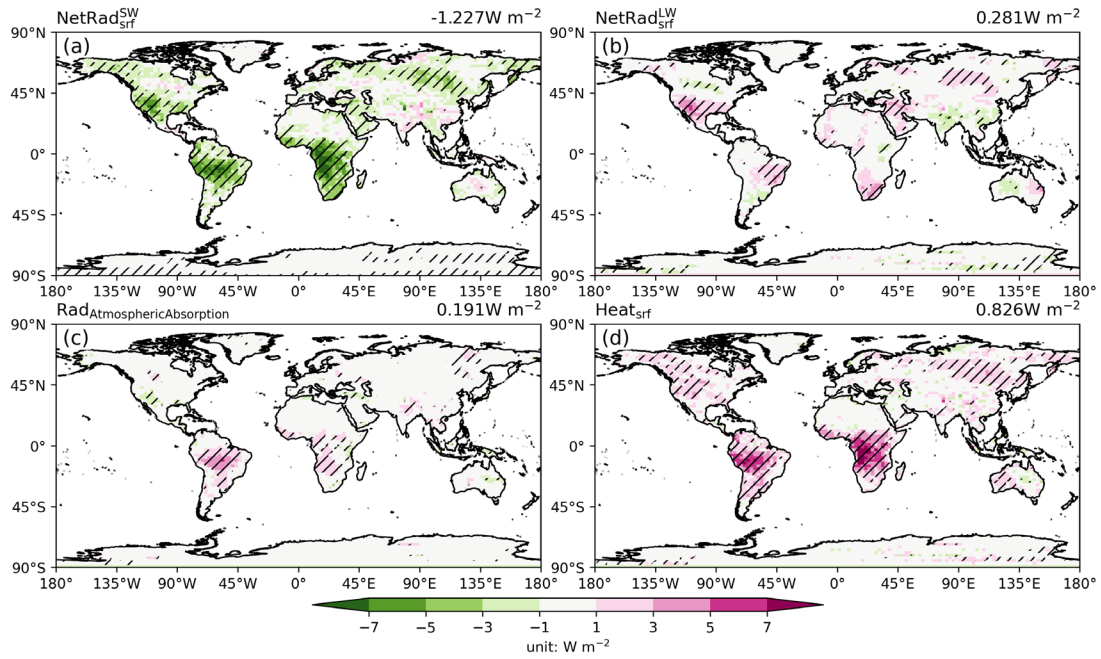
644 Yue X and Unger N 2015 The Yale Interactive terrestrial Biosphere model version 1.0: description,

645 evaluation and implementation into NASA GISS ModelE2 *Geosci. Model Dev.* **8** 2399-417
646 Yue X and Unger N 2018 Fire air pollution reduces global terrestrial productivity *Nature*
647 *Communications* **9** 5413
648 Zhuravleva T B, Kabanov D M, Nasrtdinov I M, Russkova T V, Sakerin S M, Smirnov A and Holben B
649 N 2017 Radiative characteristics of aerosol during extreme fire event over Siberia in summer
650 2012 *Atmos. Meas. Tech.* **10** 179-98
651 Zou Y, Wang Y, Qian Y, Tian H, Yang J and Alvarado E 2020 Using CESM-RESFire to understand
652 climate–fire–ecosystem interactions and the implications for decadal climate variability *Atmos.*
653 *Chem. Phys.* **20** 995-1020
654
655



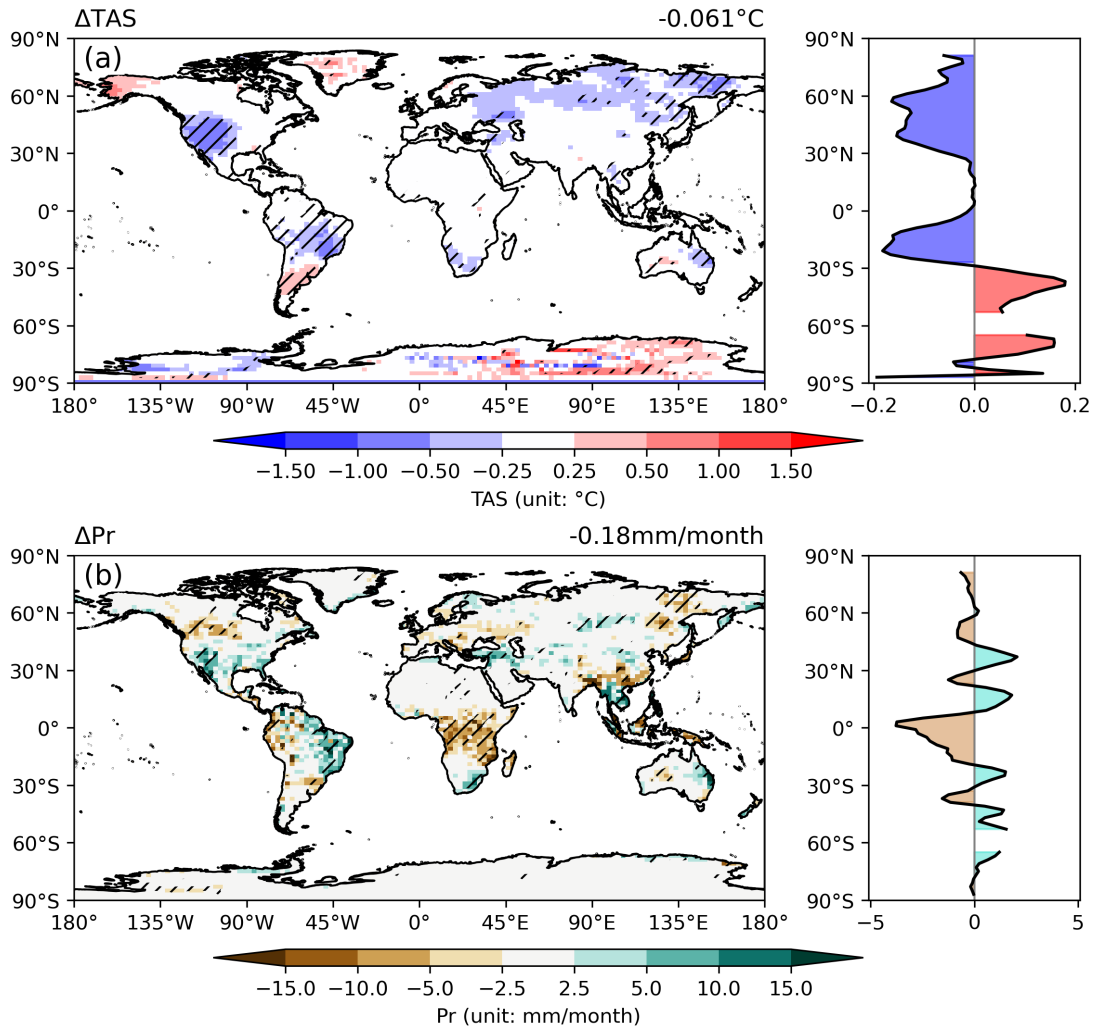
656
 657
 658
 659
 660
 661

Fig. 1 Changes in net radiation flux at top of atmosphere due to (a) total effects, (b) ADE, (c) AIE, and (d) AAE of fire aerosols. Positive values represent the increase of downward radiation. Global average value is shown at the top of each panel. Slashes denote areas with significant ($p < 0.1$) changes.



662

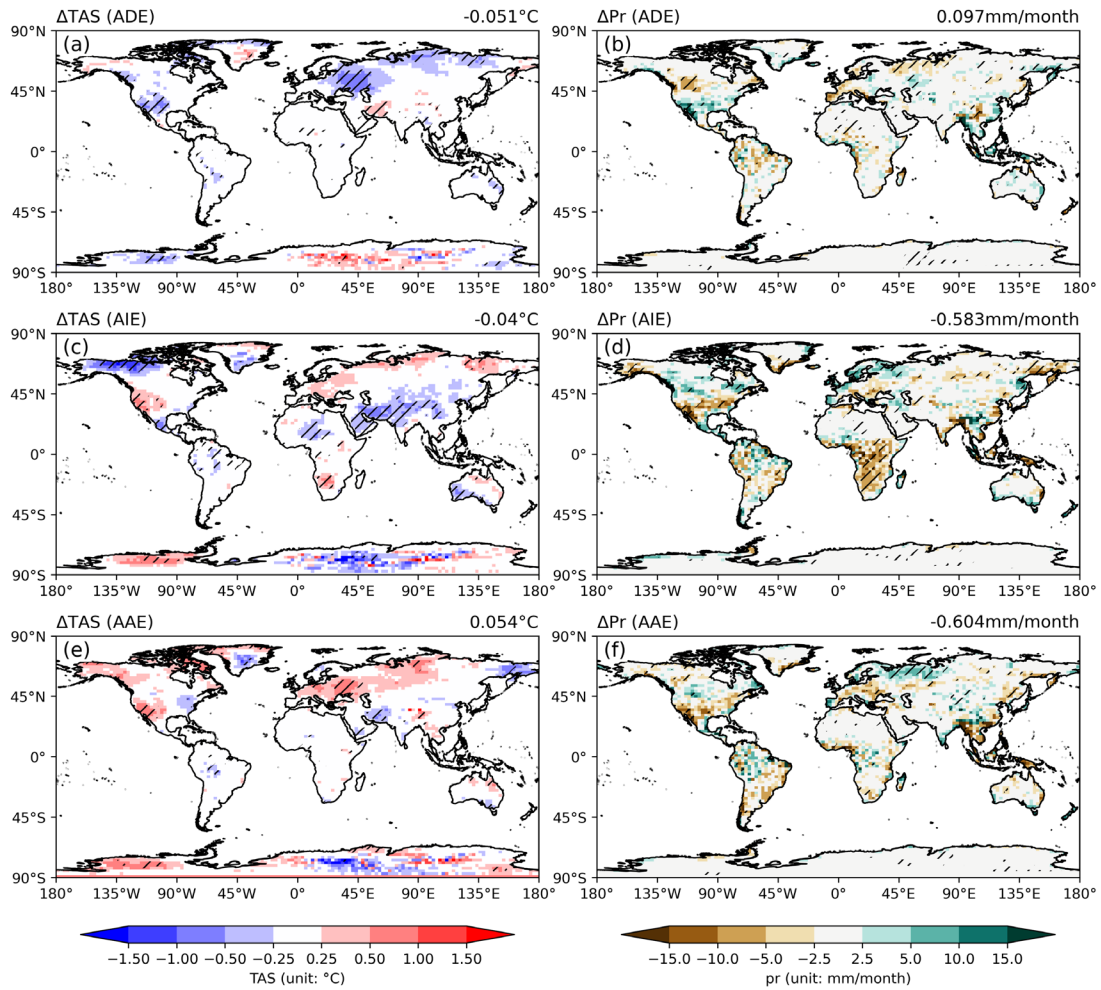
663 **Fig. 2** Changes in (a) surface net shortwave radiation, (b) surface net longwave radiation, (c)
 664 atmospheric absorbed radiation, and (d) surface heat flux (sensible + latent) over land grids caused
 665 by fire aerosols. Positive values represent the increase of downward radiation/heat for (a, b and d)
 666 and absorption for (c). Global land average value is shown at the top of each panel. Slashes denote
 667 areas with significant ($p < 0.1$) changes.
 668



669

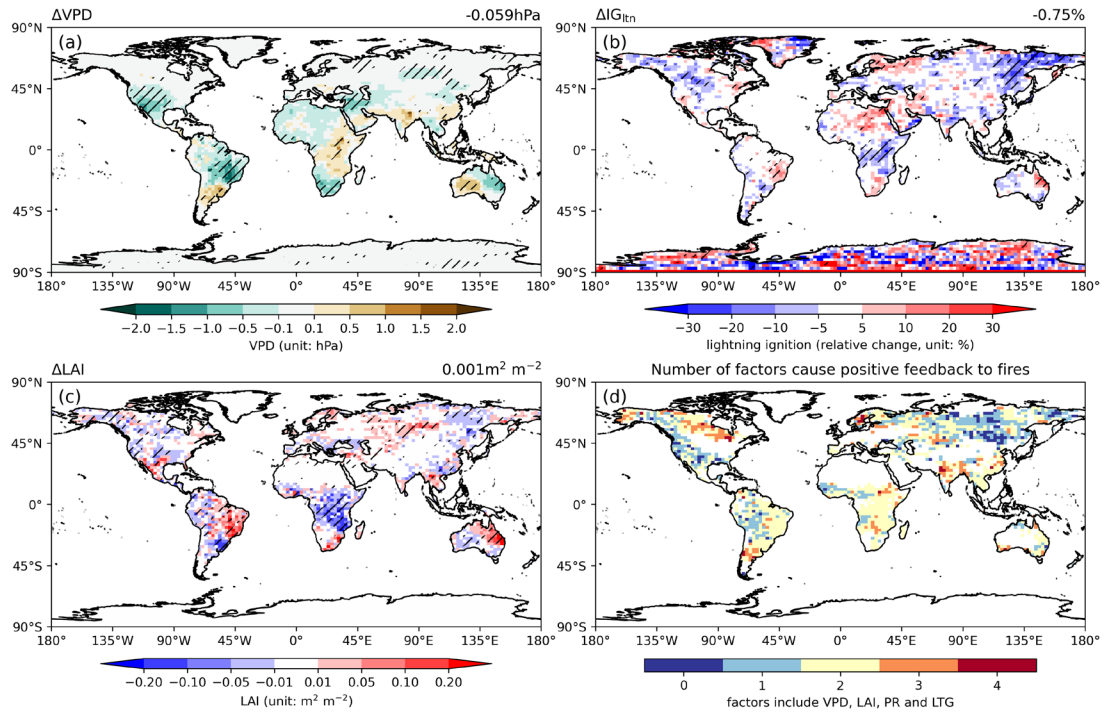
670 **Fig. 3** Changes in (a) surface air temperature and (b) precipitation over land grids caused by fire
 671 aerosols. The zonal averages of these changes are shown by the side of each panel. Global land
 672 average value is shown at the top of each panel. Slashes denote areas with significant ($p < 0.1$)
 673 changes.

674



675
 676
 677
 678
 679

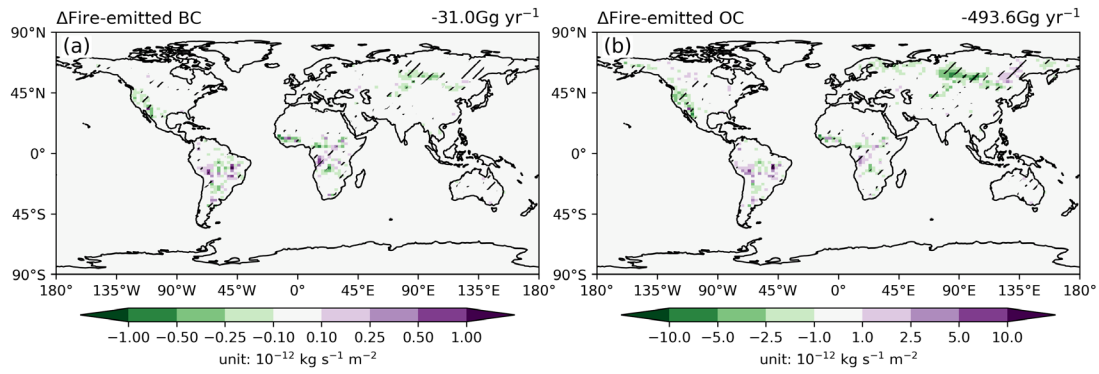
Fig. 4 Changes in (a, c, e) surface air temperature and (b, d, f) precipitation over land grids due to (a, b) ADE, (c, d) AIE, and (e, f) AAE of fire aerosols. Global land average value is shown at the top of each panel. Slashes denote areas with significant ($p < 0.1$) changes.



680

681 **Fig. 5** Changes in (a) vapor pressure deficit (VPD), (b) lightning ignition, and (c) leaf area index
 682 (LAI) over land grids induced by fire aerosols. Global land average value is shown at the top of
 683 each panel. Slashes denote areas with significant ($p < 0.1$) changes. The number of factors whose
 684 changes induced by fire aerosols cause positive feedback to fire emissions is shown in (d). Only
 685 grids with fire-emitted OC larger than $1 \times 10^{-12} \text{ kg s}^{-1} \text{ m}^{-2}$ (colored domain in Fig. S1b) are shown in
 686 (d).

687



688

689 **Fig. 6** Changes in fire emissions of (a) BC and (b) OC ~~through fire-climate interactions due to the~~
 690 ~~fast response feedback~~. The changes of fire emissions are calculated as the differences between
 691 YF_AD_AI_AA and NF_AD_AI_AA with slashes indicating significant ($p < 0.1$) changes. The
 692 total emission is shown at the top of each panel.

693

Table 1. Summary of simulations using ModelE2-YIBs

Simulation	Fires ^a	Aerosol direct effect	Aerosol indirect effect	Aerosol albedo effect
NF_AD	No	Yes	No	No
YF_AD	Yes	Yes	No	No
NF_AD_AI	No	Yes	Yes	No
YF_AD_AI	Yes	Yes	Yes	No
NF_AD_AA	No	Yes	No	Yes
YF_AD_AA	Yes	Yes	No	Yes
NF_AD_AI_AA	No	Yes	Yes	Yes
YF_AD_AI_AA	Yes	Yes	Yes	Yes

694

695 ^a All simulations predict fire emissions but the runs with NF do not feed the fire aerosols into the
696 model to perturb radiative fluxes.

697

698
699

Table 2. Comparison of the simulated fire-induced change in radiative forcings at TOA and surface climate with previous studies

Reference	RF (W m ⁻²)	ADE (W m ⁻²)	AIE (W m ⁻²)	AAE (W m ⁻²)	TAS (°C)	Pr (mm month ⁻¹)
Ward <i>et al.</i> (2012) ^a	-0.55	0.10	-1.00	0.00	—	—
Heald <i>et al.</i> (2014)	—	-0.19	—	—	—	—
Veira <i>et al.</i> (2015)	—	-0.20	—	—	—	—
Grandey <i>et al.</i> (2016)	-1.0	0.04	-1.11	-0.1	—	-0.018
Jiang <i>et al.</i> (2016)	-0.51	0.16	-0.70	0.03	-0.03	-0.3
Zou <i>et al.</i> (2020)	-0.59	-0.003	-0.82	0.19	—	—
Xu <i>et al.</i> (2021)	-0.73	0.25	-0.98	—	-0.17	-1.2
Yan <i>et al.</i> (2021)	-0.62	0.17	-0.74	-0.04	0.03	—
This study	-0.565	-0.058	-0.440	-0.016	-0.061	-0.180

700

701 ^a other effects of fire-induced on radiative turbulances are considered in this paper